A new biaxial apparatus for tensile tests on Poly Ethylene Terephthalate optimized specimen at stretch blow molding conditions

Yun Mei Luo, Thanh Tung Nguyen, Hanane Attar, Luc Chevalier, François Lesueur

Version of Record: https://www.sciencedirect.com/science/article/pii/S0142941822001994
Manuscript_05e336e3ab852b0b769ae6056ed28556

A New Biaxial Apparatus for Tensile Tests on Poly Ethylene Terephthalate Optimized Specimen at Stretch Blow Molding Conditions

Yun-Mei Luo[1], Thanh Tung Nguyen[1,2], Hanane Attar[1], Luc Chevalier*[1], François Lesueur[2]

1. Université Paris-Est, Laboratoire Modélisation et Simulation Multi Echelle, MSME UMR 8208 CNRS, 77454 Marne-la-Vallée, France

2. SIDEL BLOWING & SERVICES, Avenue de la Patrouille de France, 76930 Octeville-sur-Mer

*corresponding author: luc.chevalier@univ-paris-est.fr

Abstract

Characterization of polymer behavior over or near the glass transition temperature in condition close to industrial process remains a scientific goal. In particular being able to manage multiaxial loading at high strain rate and large strains is particularly interesting to understand Poly Ethylene Terephthalate (PET for short) behavior at condition near to the blowing process. In this paper, we present a new vertical biaxial tensile machine that has been designed and built up in our laboratory. In particular, (i) thermal regulation enables a fast and homogeneous heating of the specimen at temperature close to T_g, (ii) strain rate up to $5s^{-1}$ can be reached and (iii) a cruciform specimen geometry has been optimized to ensure large biaxial strain up to 2 or more in each direction. These two last are lower but close to the strain rate and elongation observed in stretch blow molding. The digital image correlation technique is used to obtain the displacement field and a thermal camera gives the evolution of the temperature field during the test. Dimension and height enables this apparatus to be transportable for mechanical tests under SAXS or WAXS. Here we present results of tests managed on PET and the identification procedure that is carried out to fit parameters of our

orthotropic thermo-visco-hyperelastic model. Results are presented, discussed and compared to previous measures obtained from apparatus that are more complex.

Keywords

Biaxial tensile test, specimen optimization, large strain and high strain rate, Digital Image Correlation, Poly Ethylene Terephthalate

A New Biaxial Apparatus for Tensile Tests on Poly Ethylene Terephthalate Optimized Specimen at Stretch Blow Molding Conditions

Yun-Mei Luo, Thanh Tung Nguyen, Hanane Attar, Luc Chevalier, François Lesueur

I. Introduction: measure of PET properties near to ISBM process conditions

Poly(ethylene terephthalate) (PET) bottles are obtained from injection stretch blow moulding (ISBM for short) process [1-3] that is conducted at a temperature slightly above the glass transition temperature T_g. This process involves multi-axial large strains at high strain rate and the choice of these conditions has an important impact on induced mechanical properties of the final bottle [4-6]. On the other hand, performance of the material PET regularly increases; investigations on the mechanical response of the material at process conditions have to be carried out in order to upgrade data for numerical simulation of the process. This identification procedure can be managed from the biaxial tensile test. Numerous studies have already proposed technical solutions to achieve biaxial tensile tests and data for polymers. Sasso et *al.* [7,8] developed a biaxial stretching test by blowing bubbles with an optical method to characterize hyperelastic rubber-like materials. Bhatnagar et *al.* [9] proposed a mechanism for biaxial tension tests that can be adapted on uniaxial tensile test machine. An alternative method for pulling samples of smooth materials is the rotating clamp, developed by Meissner [10] then improved by Meissner and co-workers [11,12] and Li *et al.* [13]. Sample is held between two pairs of rotating gears or cylinders. Meissner and co-workers [14,15] proposed an adaptation with 8 rotating clamps to manage equal-biaxial elongation at constant strain rate. This original design remains complex, as the one developed by Kawabata and Kawai [16] close

to the apparatus developed by Menary et al. [17]. More recently, Ru et *al.* [18] built up a low-cost biaxial tensile test device for large deformation in cruciform specimen for polymer materials. However, this device without heating system provides strains lower than 60%.

In the particular case of PET, Chandran and Jabarin [19,20] reported that for biaxial drawing of extruded PET sheet in the temperature range of 80–110°C and up to strain rate of 2 s^{-1}. Gorlier *et al.* [21] managed the uniaxial tensile test in a hydraulic Instron machine with strain rate up 0.01 s^{-1}. Chevalier and Marco [22] used tri-axial tension/compression testing machine designed in Laboratory LMT Cachan to manage biaxial tensile tests near T_g with a range of strain rates from 0.02 to 2.5 s^{-1}. Buckley and Jones [23] used a specially developed testing machine named Flexible Biaxial Film Tester to carry out the biaxial tests at temperatures 75–120°C and strain-rates 1–16 s^{-1}. Experimental uniaxial and biaxial tests performed on PET were also carried out by Menary *et al.* [17] in Queen's University Belfast. These tensile tests were managed with various speeds (from $1s^{-1}$ to $32s^{-1}$). However, these devices are horizontal and too heavy to be transportable in order to manage the test in other environment, for example, in situ biaxial test under X ray. More, these apparatuses are often complex in order to obtain a homogeneous strain field.

In this paper, we present, in section two, a vertical biaxial testing machine including heating system that has been built up at the Laboratory MSME. The simple design of the machine consists of four independent actuators and load sensors are provided along each arm for the force measurement. The biaxial tensile test managed on cruciform specimen is performed. A high-speed camera is placed to record deformation during tests and analysed using a Digital Image Correlation (DIC for short) technique. The geometry of specimen is studied in order to obtain a large strain. Since last decade, biaxial tests on flat cross-shaped specimens, with various geometries of the central zone, have already been performed for characterization of yield criteria or for identification of strain hardening model. Most of these works concerns metallic material and are focused on small strains. Muller *et al*. [24] have used a cruciform specimen with notches at intersections of arms. The shape was optimized by varying the intersection parameters to obtain a large zone of homogeneous deformation and high

strain level. Inspired from Teaca's work [25], the cruciform specimen with metal was designed with holes near the actuator to limit the slippage problem. In order to solve the rigidity problem in the central part, Makinde *et al*. [26] have presented a thickness reduction in the central zone of the cruciform specimen with metal and composite material in order to obtain maximum strain in the central zone. From then on, many researchers adopted the reduced thickness in the central zone for their specimen [27-29]. Green *et al*. [30] developed the work of Makinde *et al*. and used an aluminium cruciform with a thickness reduced central zone and seven parallel slots in each arm to maintain the deformation as uniform as possible in the gauge section. Van Paepegem's team [31-33] optimized the reduced central zone to achieve uniform biaxial failure in the centre of the specimen and minimise undesirable phenomena. Inspired of all these works, we have adapted our biaxial specimen geometry to the purpose of polymers behaviour near T_g in order to provide very large biaxial strain (up to 200%) during equal-biaxial tensile tests.

In section three, equal-biaxial tensile tests results are presented for three different temperatures (90, 100, 110°C) and three elongation speeds (25, 100, 200mm/s). The results are then used to identify the model developed for ISBM simulation. The original way to get strain from the measured displacement of the arms, and the way to get biaxial stress from measured forces is also presented and finally, the identification procedure is conduct to determine the parameters of the visco hyperelastic (VHE) model chosen for the PET behavior in ISBM conditions [34-36]. This VHE model takes into account the strain hardening and strain rate effects. This approach is compared to biaxial results managed on a different biaxial apparatus and previously presented in [39] and differences are discussed.

II. Experimental: Biaxial testing machine and specimen optimization

In this section, we present the design and development of the biaxial testing machine of our laboratory. During the stretching blow process, the maximum elongation from preform to bottle can be reached 3 to 4 times along the longitudinal and hoop direction. In order to obtain large strain of

the same order and as homogeneous as possible during biaxial tensile test, the geometry of specimen needs to be studied.

II.1. Biaxial testing machine

The biaxial testing machine was built, assembled and tested in the MSME laboratory in the nearly 2020 (Fig. 1). The main objective of this design was to be able to carry out biaxial stretching tests with large strain, with high strain rate and regulated temperature. Another constraint was the size of the device: it should remain small enough to be easily transportable in order to manage the test in other environment, for example in situ biaxial test under X ray.

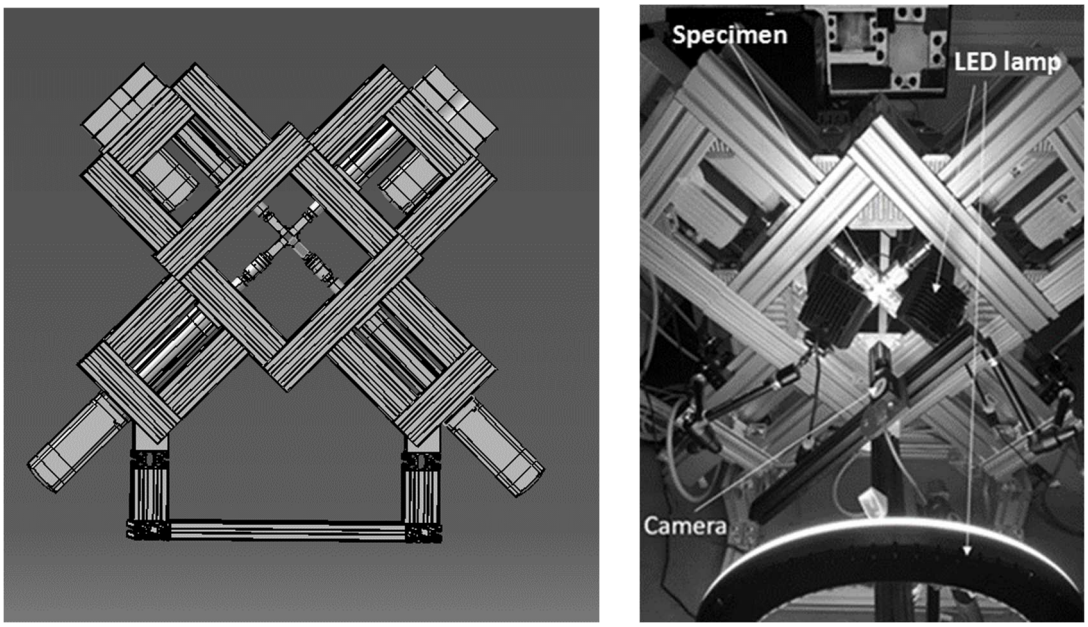

Figure 1: *Biaxial testing machine: CAD version (left) and picture of the equipped machine for ambient temperature biaxial tests*

Consequently, the dimensions of this machine are 1.2m height and 1.0m wide, its weigh is approximately 200kg. Four drives (CMMP-AS-C5-11A-P3-M0) which control four motors (EMMS-AS-100-M-HS-RMB), each connected to an electrical actuator (ESBF-BS-63- 100 -10P) from FESTO are used as the main structure of the system. These four actuators can provide independently tension or compression speeds up to 530mm/s and the maximum elongation is 200mm via two face to face actuators. With these conditions, if one uses a 40x40mm^2 specimen, elongation up to 5 could be

obtained as well as strain rate up to 26.5s^{-1}. Biaxial tensile tests that are close to the stretch blow molding process may then be conducted. A cruciform sample is used and connected to four Festo electric actuators which are piloted independently with LABVIEW software via the Modbus TCP/IP protocol. The LABVIEW software is used to control the actuators but also to provide data acquisition of the tensile forces. Between each actuator and the specimen grip, a force sensor is installed. In addition, a high-speed camera is used to capture image for DIC.

II.2. Thermal regulation

Since the stretch blow molding process is managed slightly above the glass transition temperature T_g of PET (80°C), a heating system is necessary to be considered in the equipment (Fig. 2a). first, to constitute a closed enclosure around the specimen, insulating plates were installed around the central frame of the machine. In addition, an aluminum plate insulates the front face of the apparatus and a glass plate is installed on the rear face in order to follow the evolution of the geometry for the strain measure. The specimen inside this isolated volume is heated by convection. A 3400 W power heat gun is used as the heat source. The maximum hot air flow is 800 l/min at a temperature of 300°C. A deflector was designed and installed at the end of the gun in order to avoid heating directly the specimen. The imposed circulation of hot air by the deflector can make the temperature uniform around the specimen (Fig. 2b).

An eclipsed window is managed in the center of the aluminum plate. The window is closed during heating of the specimen, but can be quickly opened to control the specimen temperature and to monitor the evolution of the temperature during the test. An infrared (IR) camera FLIR B250 is used to measure the temperature distribution of the specimen. The camera's wavelength range is 7.5–13μm and is used to follow the evolution of the preform during the fast biaxial tensile test. The PET material is opaque under the wavelength in the range of 8–12μm. The assumption is made of a constant emissivity value for this temperature level. Once the test temperature is reached, the window will be open for 3 to 5s for the test.

Thanks to the low thermal diffusivity of the polymer, the decrease of the temperature of the specimen during the window opening is very small (less than 1°C) and can be negligible. The IR camera will record the evolution of the temperature of the specimen during stretching in order to quantify the self-heating phenomena.

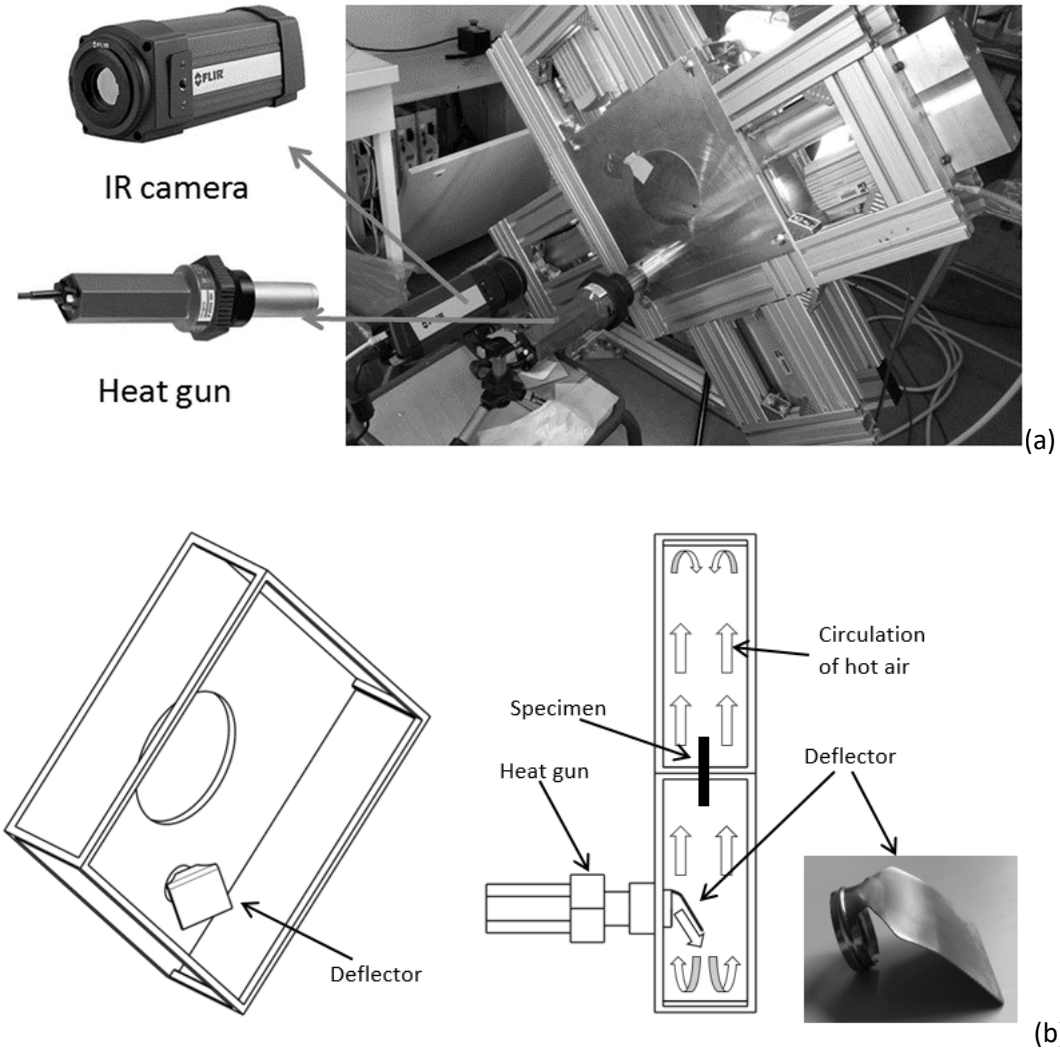

Figure 2: *Heating system, (a) view of the closed machine with the heating system and (b) isometric view of the chamber, side view of the chamber and circulation of the hot air. The picture shows the geometry of the deflector*

The camera can only monitor the temperature of one side of the specimen, but preliminary measurements carried out by thermocouples installed at different locations in the device show that difference of the temperature between the two sides of the specimen is almost zero. Figure 3a shows the temperature of the ambient air around the specimen (T1), the temperature of the surface

of actuator (T2), the temperatures of a corner point on the front side of specimen (T3 and T5) and the temperature of the center point on the front side of specimen (T4). It takes 7 to 8 minutes to reach the required temperature.

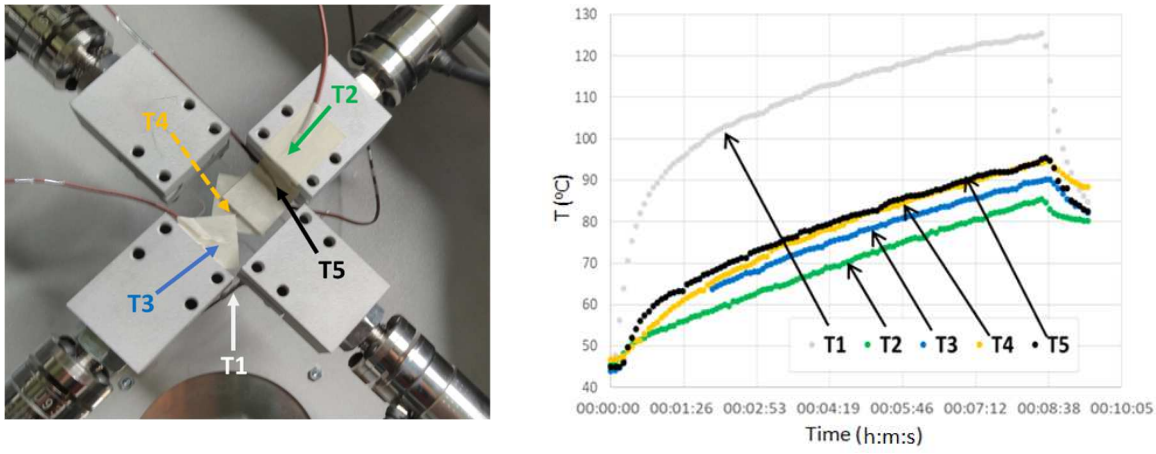

Figure 3: *Temperature evolution over time measured by thermocouples (a) different locations of the front side (b) comparison between the front and the rear side*

Figure 3b shows the comparison of the temperature of the two sides of the specimen: T4 for the front side and T5 for the rear one. One can easily see that there is no difference between these two temperatures: the deflector allows a circulation of hot air which makes a homogeneous heating. To make sure the temperature is also equal through the thickness we provide 1D numerical simulation: first we identified the convective exchange factor *h* in order to reproduce the surface temperature from the measured ambient temperature. Figure 4 left shows that the surface temperature is well represented and comparing the mid plane temperature with the external ones, it can be shown that

the difference rise up to 2° in the beginning of the heating process but quickly decreases to less 0.2°: the temperature can be considered uniform through the thickness.

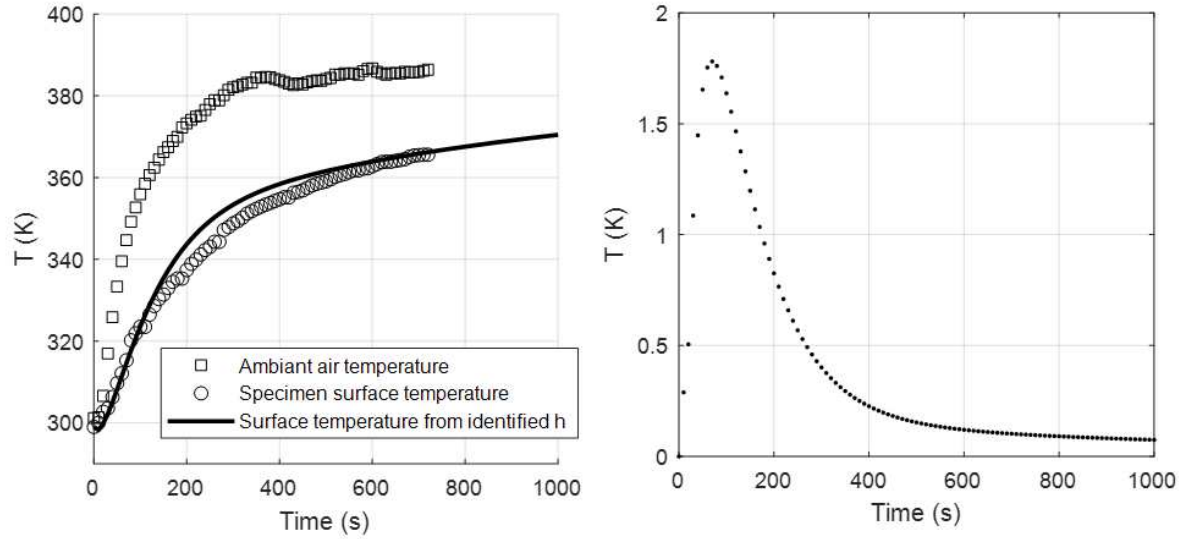

Figure 4: *Left, identification of convection parameter h from ambient temperature using 1D finite simulation. Right, difference of temperature between surface and mid plane of the specimen obtained from 1D simulation in thickness.*

The temperature is also uniform over the entire studied area of the specimen is verified by the IR camera (Fig. 5). The difference of the temperature on the two diagonal lines of the specimen is less than 2°C. The thermal regulation allows us to carry out equal-biaxial tensile tests at different temperatures characteristic of the ISBM process (90, 100 and 110°C).

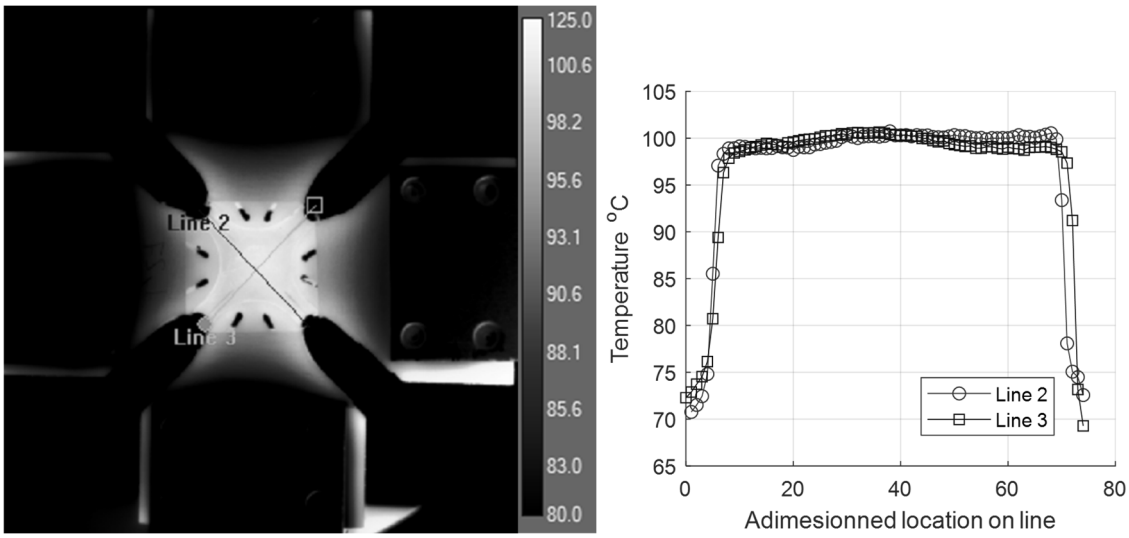

Figure 5: *Temperature distribution on the specimen, uniform temperature covers the central zone of the specimen (left) and temperature plot for the two diagonal lines (line 2, line 3) for 100°C imposed.*

II.3. Biaxial specimen optimization

It is not easy to reach large biaxial elongations (more than 3) with a cross-shaped specimen because of the rigidity of the central zone: under an identical thickness and temperature, arms are easier to stretch uniaxially rather than the center biaxially. Consequently, for a given displacement of the actuators, biaxial strains remain small and only the arms are stretched. Therefore, an optimization of the specimen geometry is needed in order to have a biaxial elongation in the center of the specimen. These strains have to be large enough to proceed the identification of mechanical behavior of PET.

Amorphous granular of PET is supplied by SIDEL group. Plates with dimensions of 125x125x4 (mm) are injected in the PIMM laboratory at *Arts et Métiers Paris*. The specimen is then cut from the plate by a water jet cutting machine. The first version of the specimen was a simple cross with constant thickness represented in Fig. 6a. Scotch tape with thermal insulating properties is stuck on the arms of the specimen to reduce their temperature during the heating stage in order to make sure that the arms are less flexible than the zone of interest. Measuring the expansion of the diagonal of the zone of interest (see Fig.6a) obtained for the same displacement of the actuators will be the indicator of the specimen performance. In this first version, with displacement equal to 30mm for each actuator, the elongation remains low: it is only 1.05 that is equivalent to a 5% strain. This could be enough to identify the elastic properties but it is clearly not enough for the identification of the behavior of PET under ISBM condition. In addition to the problems of the rigidity of center part, sliding also occurs of the arms of specimen in the grips.

In order to solve the sliding problem, the second version was inspired from the specimen of Teaca's work [25]. With the four screws of each grip, the second version consists of large arms and holes for the screw passage (see Fig. 6b) so that slippage is limited. The biaxial strain has increase with this

first improvement but still remains insufficient: the elongation of the diagonal goes to 1.3 that is equivalent to 30% strain.

(a) 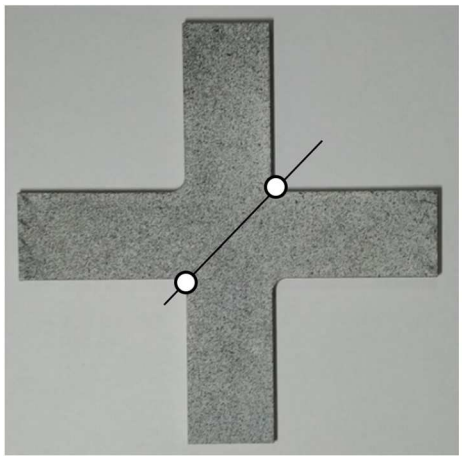 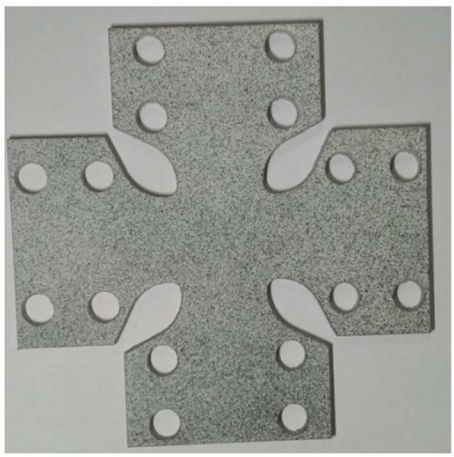 (b)

Figure 6: *(a) initial cruciform specimen; (b) second version of specimen*

Inspired by Green's work [30], several versions of specimen were tested with a thickness reduction in the central zone to reduce the rigidity and obtain a maximal biaxial strain. The thickness of the central zone is thinned by a high-speed milling machine on the two faces of the specimen in order to keep the plane medium as the symmetry plane. Adding two slits in each arm helps to maintain the strain field as uniform as possible in the studied zone. The slits make the arms more flexible in the transverse direction but remain rigid in the tensile direction compared to the central zone.

Figure 7 shows the initial shape and the deformed shape of the two first version (Fig.7a and b) and the optimized version (Fig.7c). The optimization of the shape of the specimen makes it possible to reach an elongation rate equal to 2 (100% strain which is clearly a large strain). This value is very large for a simple biaxial tensile machine but remains lower compared to stretch blow process. Nevertheless, the following section will show that this is enough for the identification procedure. More, since there is a large homogenous deformed zone in the studied area of specimen, it is possible to make assumptions that will facilitate the identification process.

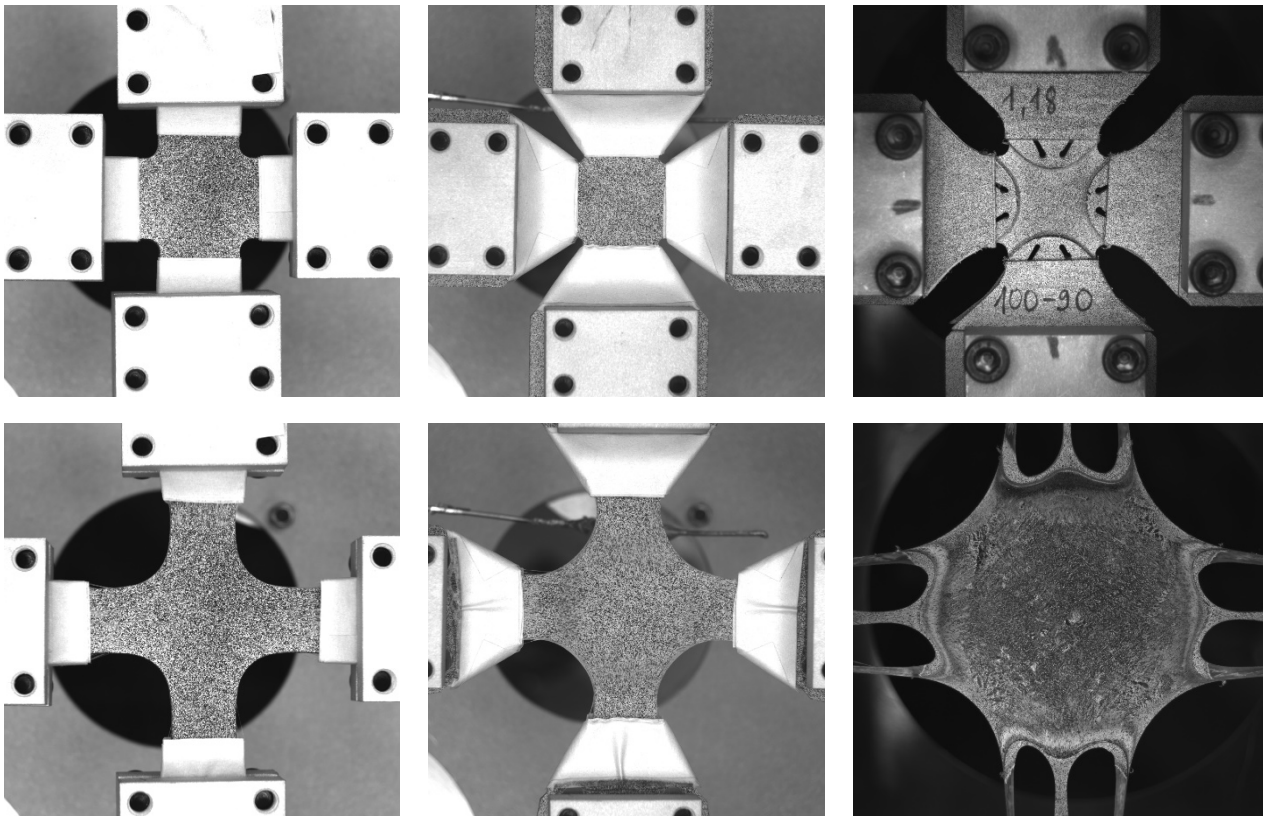

(a) $\lambda = 1{,}05$ *(b)* $\lambda = 1{,}3$ *(c)* $\lambda = 2$

Figure 7: *Diagonal elongation for different version shape of the specimen: (a) initial version; (b) second version; (c) last version*

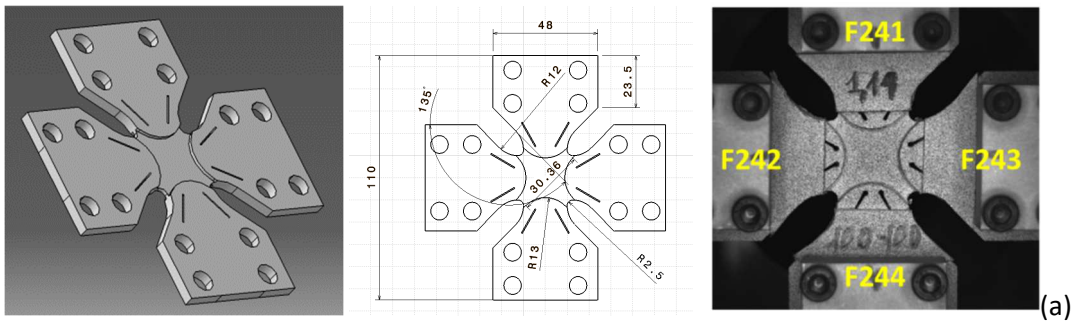

(a)

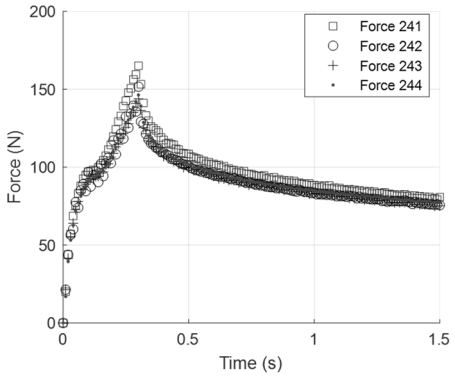

(b)

Figure 8: *(a) Optimized geometry of specimen; (b) force evolution versus time for a speed 100mm/s*

Figure 8a shows several views of the optimized specimen. Figure 8b shows the evolution of the load versus time which are recorded by the sensors. In this case, the specimen is heated up to 100°C and stretch speed is 100mm/s. Under an equal-biaxial tensile test, the traction lasts 0.3s and the typical strain hardening effect of PET appear. One can notice that the evolution of the four forces is identical and that is characteristic of a well-balanced test.

III. Results and discussion: identification of the VHE model for PET near ISBM conditions

The displacement field is captured by a camera through the glass plate on the back side of the device. The camera can record 100 images/s. The images are then studied and managed by the DIC Correli^{GD} software. At the same time, the sensors record the force values versus time. We use these information to calculate both biaxial strain and stress in the central region of the specimen. Dilatation occurs during the heating stage but since the thickness of the central zone is really thin the sample bends a little but no compression occurs. When the test begins, a very short delay appears before the load begins to increase and the time "zero" is chosen at this specific beginning. Pictures are taken regularly and the reference picture for the DIC analysis is the one taken at time "zero".

III.1. Biaxial stress-strain curves determination

III.1.1 Biaxial strain calculation

Figure 7c represents the initial and final geometry of one of the biaxial tests: the measurement of the final diagonal compared to the initial diagonal gives an elongation L/L_o is more or less equal to 2 (i.e. deformation in the 45° direction of 100 %). It is clearly a large deformation but smaller than those encountered in the blowing process.

A measurement of the lengths of the diagonals shows that the evolution of the length $L(t)$ is well represented by an affine law versus the displacement $U(t)$ of the jaws as shown in Fig. 9. Thus, if we assume that the deformation field is sufficiently homogeneous over the study area, we may be

tempted to consider that the biaxial deformation can be calculated simply from the displacement of the grips.

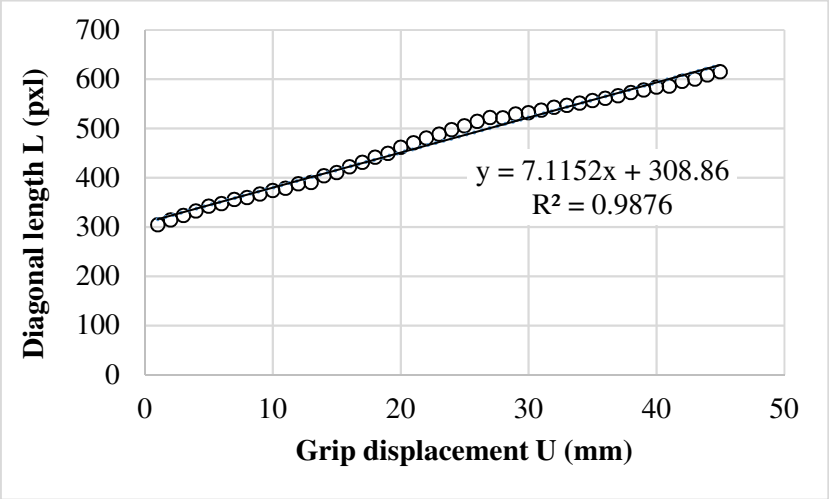

Figure 9: *Evolution of the diagonal AB length L(t) during the biaxial test versus the grips displacement U(t) at 100mm/s and 90°C*

Times *t* varies from 0 to 0.45s and, in the meantime, *U* varies from 0 to 45mm. Length *L* is given in pixel. Unfortunately, this linearity fails if one uses the DIC to analyze the strain fields ε_{xx}, ε_{xy} and ε_{yy}.

Figure 10 shows that (i) the central zone is 250% stretched and that (ii) the displacement field generates elongations that vary along the diagonal. One can visualize that the initial square grid becomes distorted along the diagonal AB. The 90° angle between the horizontal axis ***X*** and the vertical axis ***Y*** opens which means that ε_{xy} takes a negative value near A and B locations. Consequently, the relative elongation in the AB direction that writes:

$$\varepsilon_{aa} = \vec{a}.\left(\underline{\underline{\varepsilon}}\vec{a}\right) = \frac{\varepsilon_{xx} + \varepsilon_{yy}}{2} + \varepsilon_{xy} \qquad (1)$$

where *a* is the unit vector along AB, decreases from the max value at the center of the specimen to the extremities A and B.

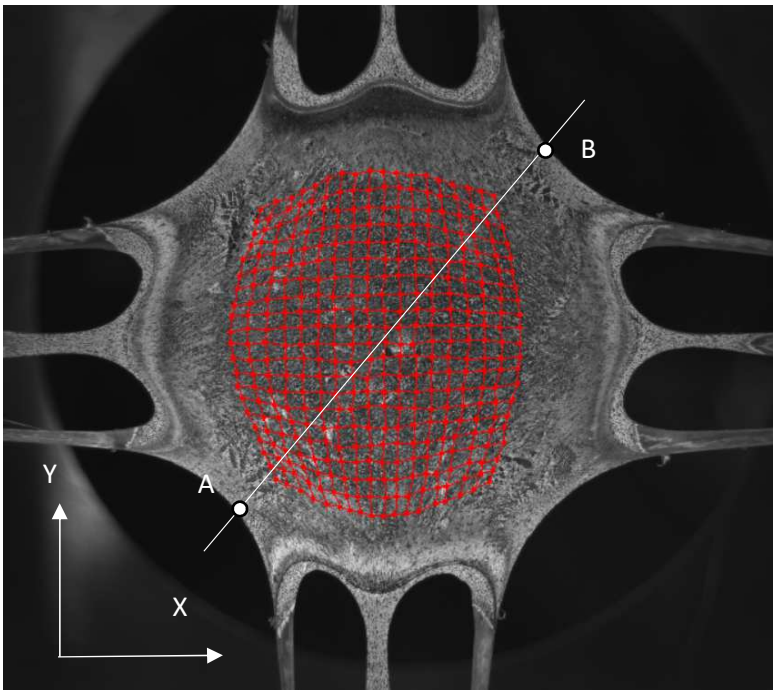

Figure 10: *Deformed grid of the biaxialy stretched sample at 100mm/s and 90°C. The grid is initially square. The squares become bigger in the central region and are distorded when approaching to the edges of the diagonal AB.*

Figure 11 shows the evolution of the ε_{aa} along AB (and along the second diagonal) versus the no-dimensional length ξ=s/L where *s* is the distance from A on the diagonal and *L* its length at time *t*. One can see that ε_{aa} is not constant; it is maximal in the center and becomes negative near the edges. The evolution is similar on both diagonals and more or less parabolic. For this case, if one calculate the ratio L/L_0 where L_0 is the initial length of the diagonal of the specimen and *L* the final length, the global elongation seems to be 2 (the diagonal length increases 100%). Using the DIC analysis one can see that the local elongation in the middle of the specimen rises up to 3.5 (ie. 250% increase of an elementary length). Consequently, the real elongation for our optimized specimen is really close to the ISBM biaxial stretching. If one plots the maximum value of ε_{aa} of the two diagonals versus the grips displacement U(t), one can see on Fig.12 that (i) the evolutions are identical and that (ii) the evolution is nearly linear from 0 to 25mm of displacement *U(t)* but this linearity disappears

then. For this reason, we use DIC tool Correli^{GD} to determine all strains in order to plot the behavior curves used for identification (3 temperatures and 3 velocities).

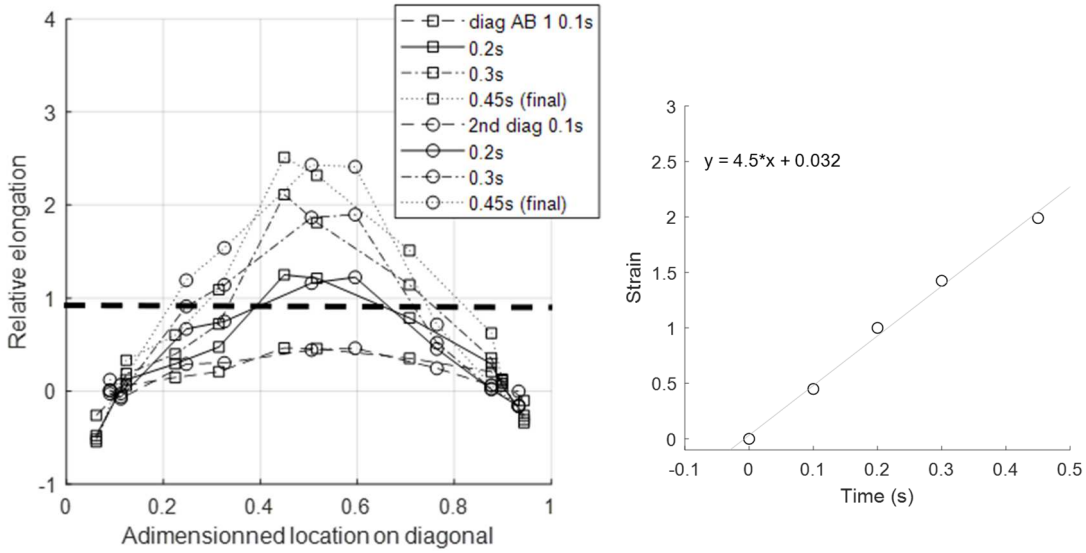

Figure 11: *Left, relative elongation ε_{aa} along the diagonal AB at several time t for the biaxial test at 100mm/s and 90°C. Right, from the central strain versus time one can identify the strain rate, here 4.5s^{-1} for 100mm/s and 90°C.*

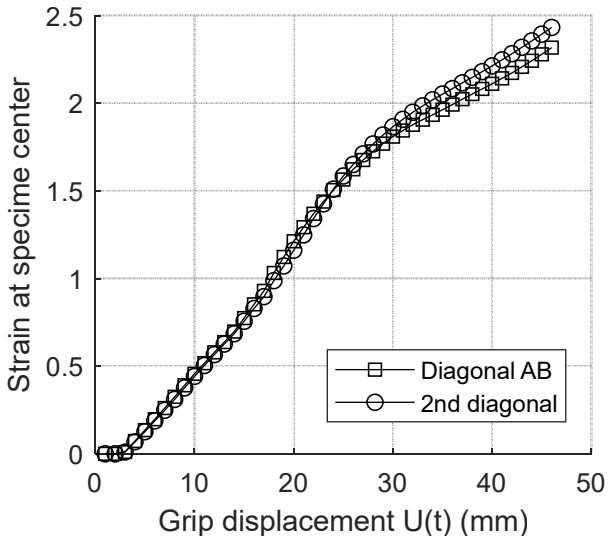

Figure 12: *Evolution the relative elongation ε_{aa} at the specimen centre for the biaxial test at 100mm/s and 90°C.*

III.1.2 Biaxial stress calculation

The relative elongation in the direction normal $\vec{n}$ to the diagonal writes:

$$\varepsilon_{nn} = \vec{n}.\left(\underline{\underline{\varepsilon}}\vec{n}\right) = \frac{\varepsilon_{xx} + \varepsilon_{yy}}{2} - \varepsilon_{xy} \qquad (2)$$

The change from the plus to the minus sign leads to an evolution of ε_{nn} completely different from ε_{aa}. Figure 13 illustrates this evolution of ε_{nn} versus ξ for different time *t*. Despite the irregularities, the evolution is more or less constant along the line and that it is possible to assume that this relative elongation is uniform. Consequently, the associated biaxial stress σ is uniform along the diagonal, as it has already been done in [22].

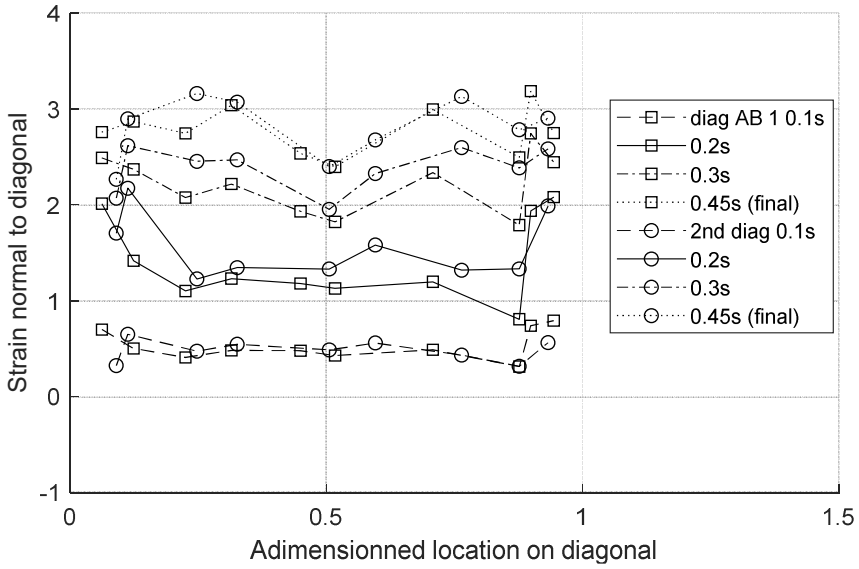

Figure 13: *Strain ε_{nn} along the diagonal AB at different time t for the biaxial test at 100mm/s and 90°C. Compared to ε_{aa} these curves look quite « uniform ».*

It is the possible to evaluate the biaxial stress from the measured force *F* using the assumption of uniform stress along the diagonal as illustrated on Fig. 14. One can obtain the expression of the stress by:

$$\sigma = \frac{\sqrt{2}F}{eL} \qquad (3)$$

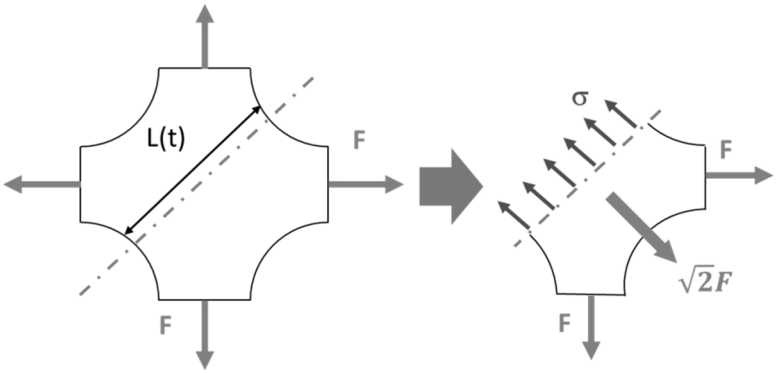

Figure 14: *Balance of the half sample for the biaxial stress calculation*

The mean thickness *e* and the length of the diagonal *L* have to be evaluated at all time *t*. If incompressibility is assumed one can evaluate the mean thickness *e* from the measure of *L:*

$$\lambda = \frac{L}{L_0} \Rightarrow \frac{e}{e_0} = \left(\frac{L_0}{L}\right)^2 = \frac{1}{\lambda^2} \tag{4}$$

that is linearly related to $\underline{U}(t)$ and lead to the stress determination from:

$$\sigma = \frac{\lambda\sqrt{2}F}{e_0 L_0} \tag{5}$$

Imposed velocity *V* to the grips gives the displacement: $U(t) = Vt$ and finally the diagonal elongation $\lambda(t)$. This process is applied for the 9 stress-strain curves presented in Fig.15.

III.2. Influence of temperature and strain rate

Equal-biaxial tensile tests were carried out for 3 different temperatures (90, 100, 110°C) and 3 stretching speeds (25, 100, 200mm/s). The maximum displacement of each actuator is 50mm (100mm for 2 sides). A set of 9 tests was carried out for each condition to ensure repeatability. Figure 15 shows that at any stretching speed, the stresses decrease when the temperature increases. This classic result is logical because the material becomes softer at higher temperature. The highest stress appears always at 90°C. When the test temperature increases, the maximum value of strain decreases. It can be explained by the flexibility of the arms of the specimen which increases with the temperature. At higher temperature, the arms are more heated and therefore they become more

flexible. On all cases, it can be seen that the hardening effect begins at the strain above 100% and this effect decreases when the temperature increases. Among these 3 speeds, the influence of temperature is more visible at 25 mm/s. The material is more sensitive to temperature than to strain rate, highlighting a behavior that is more hyperelastic than viscous.

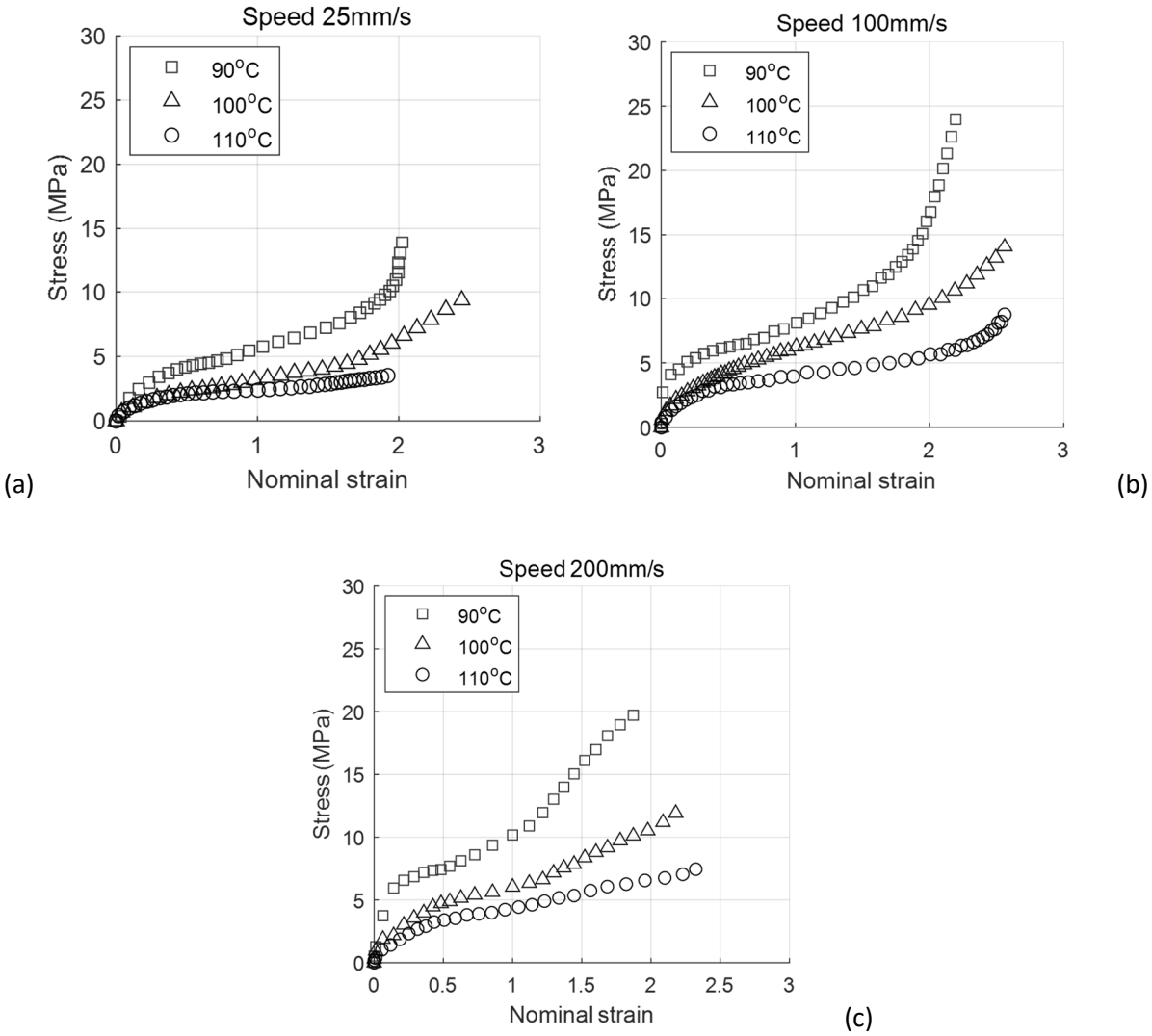

Figure 15: *Experimental stress-strain curve under different temperature (a) tension speed 25mm/s; (b) tension speed 100mm/s; (c) tension speed 200mm/s*

Figure 16 shows the different mechanical response for PET during the recent 15 years. Under similar experimental conditions: temperature at 90°C and strain rate between $2s^{-1}$ and $4s^{-1}$, higher performance of PET is obtained from Menary *et al.* [17] than the one in the Chevalier and Marco's work [22] which is earlier research. This PET material highlights a strongest response than in previous works that confirms the necessity to upgrade the mechanical parameter for ISBM simulation of PET.

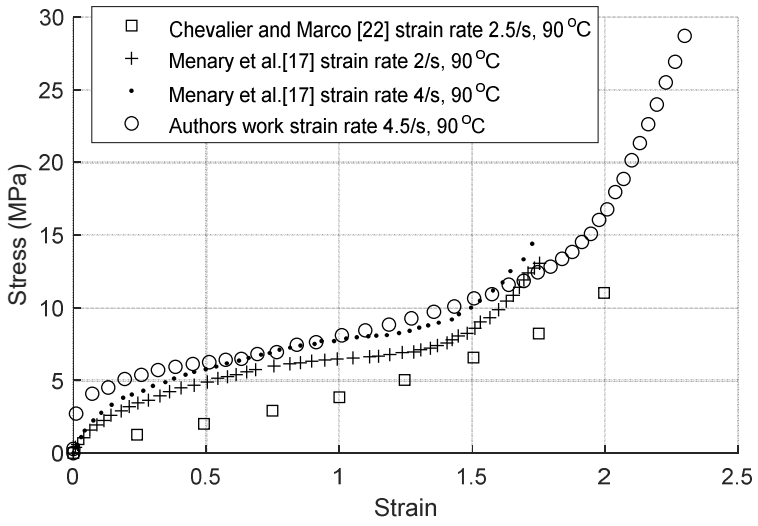

Figure 16: *Comparison of different mechanical response for PET*

In authors' previous work [39], the measured elastic properties of PET bottles are more than 1.3 times higher than they were 10 years ago. When the nominal strain is lower than 1, the stress-strain curves are coincident for Menary *et al.* and this work, both are higher than Chevalier and Marco's results.

III.3. VHE model identification

III.3.1 VHE model presentation

In author's previous work [34-36], an orthotropic thermal dependent visco-hyperelastic (VHE) model has been proposed and identified. For elastic part, a Hart Smith type hyper elastic model is considered. On the other hand, for viscous part, an incompressible nonlinear model including viscous strain and viscous strain rate is used. The elastic and viscous expressions of the deviatoric part of the stress tensor $\underline{\underline{\hat{\sigma}}}$ in the model can be written in the following way:

Elastic part:

$$\underline{\underline{\hat{\sigma}}} = 2G_1 e^{\Lambda_1 (I_1-3)^2} \underline{\underline{\hat{B}_e}} + 2I_4 G_2 e^{\Lambda_2 (I_4-1)^2} \underline{\underline{\hat{A}_1}} + 2I_6 G_2 e^{\Lambda_2 (I_6-1)^2} \underline{\underline{\hat{A}_2}} \quad (6a)$$

Viscous part:

$$\underline{\underline{\hat{\sigma}}} = 2\underline{\underline{\underline{\underline{\eta}}}} \underline{\underline{D_v}}$$

or

$$\begin{pmatrix} \hat{\sigma}_{11} \\ \hat{\sigma}_{22} \\ \sqrt{2}\sigma_{12} \end{pmatrix} = 2\begin{bmatrix} \eta_{11} & \eta_{12} & 0 \\ \eta_{12} & \eta_{22} & 0 \\ 0 & 0 & \eta_{44} \end{bmatrix}\begin{pmatrix} D_{v11} \\ D_{v22} \\ \sqrt{2}D_{v12} \end{pmatrix} \tag{6b}$$

where $\underline{\underline{B_e}}$ the elastic left Cauchy Green tensor; G_1, G_2, Λ_1 and Λ_2 are parameters of the elastic part; $\hat{\underline{\underline{B_e}}}$ the deviatoric part of $\underline{\underline{B_e}}$; I_1 the classical invariants of $\underline{\underline{B_e}}$, I_4 and I_6 are the invariants associated to the orthotropic behavior:

$$I_1 = tr\left(\underline{\underline{B_e}}\right), \quad I_4 = \underline{n_1} \cdot \underline{\underline{B_e}} \cdot \underline{n_1}, \quad I_6 = \underline{n_2} \cdot \underline{\underline{B_e}} \cdot \underline{n_2} \tag{7}$$

$\underline{n_1}$ and $\underline{n_2}$ are the privileged directions for orthotropic properties. $\underline{\underline{A_i}}$ the second order structural tensors of the preferred directions:

$$\underline{\underline{A_1}} = \underline{n_1} \otimes \underline{n_1}, \quad \underline{\underline{A_2}} = \underline{n_2} \otimes \underline{n_2} \tag{8}$$

In viscous part, an incompressible nonlinear form is proposed. D_v in Eq.6b is the viscous strain rate; h_i the specific functions which depend on viscous strain for each orthotropic direction:

$$\begin{cases} \eta_{11} = \eta_0(T)\, h_1 f\left(\overline{\dot{\varepsilon}_v}\right) \\ \eta_{12} = \eta_0(T) \max\left(h_1, h_2\right) f\left(\overline{\dot{\varepsilon}_v}\right) \\ \eta_{22} = \eta_0(T)\, h_2 f\left(\overline{\dot{\varepsilon}_v}\right) \\ \eta_{44} = \eta_0(T) \max\left(h_1, h_2\right) f\left(\overline{\dot{\varepsilon}_v}\right) \end{cases} \tag{9}$$

with:

$$\begin{cases} h_1 = \left(1 - \exp\left(-K\varepsilon_{v1}\right)\right) \cdot \exp\left(\alpha_1\left(\dfrac{\varepsilon_{v1}}{\varepsilon_{vref}(T)}\right)^2 + \alpha_2\left(\dfrac{\varepsilon_{v1}}{\varepsilon_{vref}(T)}\right)\right) \\ h_2 = \left(1 - \exp\left(-K\varepsilon_{v2}\right)\right) \cdot \exp\left(\alpha_1\left(\dfrac{\varepsilon_{v2}}{\varepsilon_{vref}(T)}\right)^2 + \alpha_2\left(\dfrac{\varepsilon_{v2}}{\varepsilon_{vref}(T)}\right)\right) \end{cases} \tag{10}$$

and:

$$f\left(\overline{\dot{\varepsilon}_v}\right)=\frac{1}{\left(1+\left(\lambda\overline{\dot{\varepsilon}_v}/\dot{\varepsilon}_{ref}\right)^a\right)^{\frac{1-m}{a}}},\overline{\dot{\varepsilon}_v}=\sqrt{\frac{2}{3}tr\left(D_v^2\right)} \tag{11}$$

$$\ln\left(\alpha_T\right)=\frac{-C_1\left(T-T_{ref}\right)}{C_2+T-T_{ref}},\ \eta_0(T)=\alpha_T\eta_0\left(T_{ref}\right) \tag{12}$$

$$\varepsilon_{vref}(T)=\frac{\varepsilon_{vref}(T_{ref})}{\exp\left(-C_3\left(T-T_{ref}\right)+C_4\right)} \tag{13}$$

where ε_{vi} the viscous elongation for each orthotropic direction; *K*, α_1 and α_2 are the parameters in h_i function; λ, *m*, *a* are parameters of the Carreau-Yasuda type function $f\left(\overline{\dot{\varepsilon}_v}\right)$. $\overline{\varepsilon_v}$ the equivalent viscous strain rate and $\dot{\varepsilon}_{ref}$ is a reference strain rate that can be taken equal to 1s^{-1}. $\eta_0\left(T\right)$ and $\varepsilon_{vref}(T)$ are 2 thermal dependent variables. Williams-Landel-Ferry (WLF) model was chosen for the evolution of $\eta_0\left(T\right)$. C_1 and C_2 are WLF parameters, T_{ref} = 90°C. C_3 and C_4 are parameters in $\varepsilon_{vref}(T)$.

III.3.2 VHE model identification

The simulation of equal-biaxial tensile test is carried out using finite element code in software Matlab. The well-known inf-sup condition or the LBB condition [37,38] guaranties the stability of a finite element velocity - pressure calculation as a quadratic interpolation for velocity and linear for pressure. By analogy, we choose a quadratic interpolation for velocity $\underline{V}$ and linear interpolation for $\underline{\underline{B_e}}$.

TABLE 1. The characteristics of the PET

$G(\varepsilon_e)$		G_1		λ_1		G_2		λ_2	
		2 MPa		1		2 MPa		1	
$\eta(\varepsilon_v, \overline{\dot{\varepsilon}_v}, T)$	$f\left(\overline{\dot{\varepsilon}_v}\right)$	λ		a		m			
		10.51		10.43		0.23			
	$h\left(\overline{\varepsilon_v}\right)$	η_0	K	α_1	α_2	α_3			
		1 MPa.s	10	10	-2.1	2			

	$\eta_0(T),\varepsilon_{vlim}(T)$	C_1	C_2	C_3	C_4 (°C)
		2.5	55.3	0.8	200

Considering the thermal effect, Mechanical and thermal balance equations are fully non-linear and solved together with implicit schemes on the current deformed configuration, which is updated at each time step. Newton-Raphson method is used to solve this nonlinear problem. 'fminsearch' in the toolbox *Matlab* is used to manage the identification. This tool can identify the characteristics of VHE model from minimizing the difference between the curves experimental and numerical simulation for different point of measurement. Table 1 lists the identified parameters of the proposed VHE model.

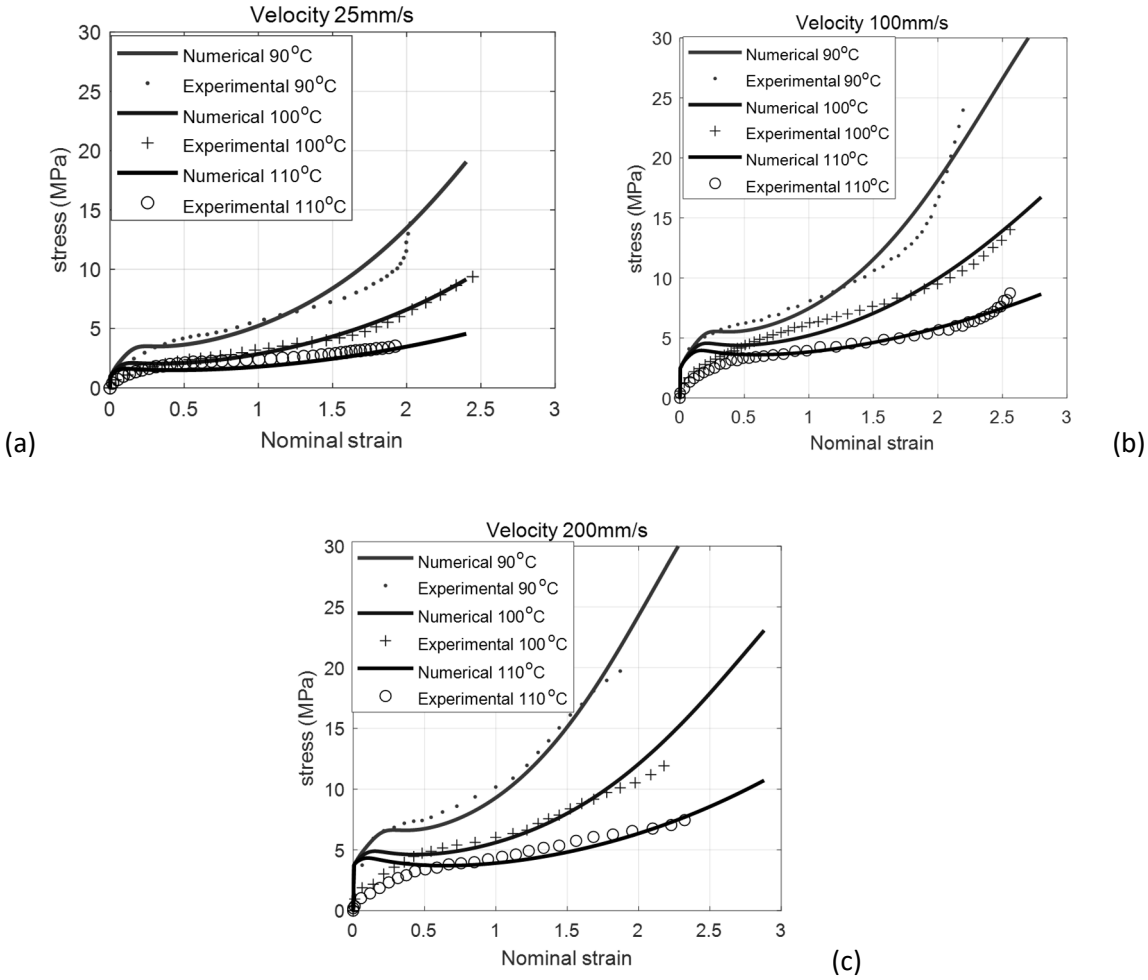

Figure 17: *Comparison between experimental results and model simulations under different temperature (a) speed 25mm/s; (b) speed 100mm/s; (c) speed 200mm/s*

Figure 17 shows the comparison between the numerical results using the identified model and the experimental equal-biaxial results. Numerical simulation gives a good representation of strain hardening effect and thermal effect. For each temperature and stretching speed, the absolute difference between numerical result and experimental one does not exceed 20%. The main difference between experimental data and numerical simulation is at the beginning of the curve: the initial slope of the experimental curves varies when the strain rate increases while it remains the same is the numerical results. This understandable since the elasticity in the model does not depend on the strain rate.

IV. Conclusions

We present a portable biaxial testing device including a heating system that can provide biaxial tensile tests close to the ISBM process condition for temperature and strain rate. The design is simple and inspired from many publications on other biaxial apparatus; the shape of our cruciform specimen has been optimized in order to obtain a large strain in the central zone. Biaxial elongation up to 3.5 in each direction can be reached with this geometry.

Using the developed shape of the specimen, equal-biaxial tensile tests under different temperature and stretching speeds were carried out. The DIC technique was conducted to justify the simple procedure used to determine the biaxial strain and stress in the central region of the specimen.

An identification procedure was carried out in order to determine the parameters of the thermo dependent visco hyperelastic (VHE) model developed at MSME for ISBM simulations. This VHE model takes into account the strain hardening and strain rate effects. Numerical simulation with the identified characteristics presents a good agreement with experimental equal-biaxial results.

Compared to previous published results of the PET behaviour at the same temperature and strain rate conditions enables to validate our identification methodology.

Acknowledgement

Authors thank SIDEL group to provide PET granular for injection and the PIMM laboratory at “Arts et Métiers” Paris (France) to provide machine and mold for injection of the amorphous PET plates. They thank LabEx MMCD and University Gustave Eiffel for financial support for the biaxial apparatus.

References

[1] F.M. Schmidt, J.F. Agassant, M. Bellet, Experimental study and numerical simulation of the injection stretch/blow molding process. Polymer Engineering and Science, Newtown Vol. 38, N° 9, 1998. https://doi.org/10.1002/pen.10310.

[2] H. X. Huang, Z. S. Yin and J. H. Liu, Visulisation study and analysis on preform growth in polyethylene terephthalate stretch blow moulding, Journal of Applied Polymer Science, vol. 103, no. 1, pp.564-573, 2007. https://doi.org/10.1002/app.25116.

[3] M. Cakmak, J.L. White, J.E. Spruiel, An investigation of the kinematics of stetch blow molding of Poly(ethylene terephthalate) bottles, J. of App. Polymer Sci., 30, 3679-3695, 1985. https://doi.org/10.1002/app.1985.070300913.

[4] B. Cosson, L. Chevalier, J. Yvonnet, Optimisation of the Thickness of PET Bottle during Stretch-Blow Moulding by using a Mesh-Free (Numerical) Method. Int. Polymer Process, 24(3), 223–233, 2009. https://doi.org/10.3139/217.2215.

[5] G. Marckmann, E. Verron, B. Peseux, Finite element analysis of blow molding and thermoforming using a dynamic explicit procedure. Polymer Eng Sci 41(3):426–439, 2001. https://doi.org/10.1002/pen.10740.

[6] J. Nixon, S. Yan, G.H. Menary, Analysis and Simulation of the Free-Stretch-Blow Process of PET. KEM, 554–557:1729–37, 2013. https://doi.org/10.4028/www.scientific.net/kem.554-557.1729.

[7] M. Sasso, D. Amodio, Development of a Biaxial Stretching Machine for Rubbers by Optical Methods, Proceedings of SEM Annual Conference, St Louis, MO, 2006.

[8] M. Sasso, G. Palmieri, G. Chiappini, D. Amodio, Characterization of hyperelastic rubber-like materials by biaxial and uniaxial stretching tests based on optical methods. Polym Test 27(8):995–1004, 2008. https://doi.org/10.1016/j.polymertesting.2008.09.001.

[9] N. Bhatnagar, R. Bhardwaj, P. Selvakumar, M. Brieu, Development of a biaxial tensile test fixture for reinforced thermoplastic composites. Polym Test 26(2):154–161, 2007. https://doi.org/10.1016/j.polymertesting.2006.09.007.

[10] J. Meissner, Rheometer zur Untersuchung der deformations mechanischen Eigenschaften von Kunststoff-Schmelzen unter definierter Zug-beanspruchung, Rheol. Acta, 878-88, 1969. https://doi.org/10.1007/BF02321358.

[11] J. Meissner, Dehnungsverhalten von Polyäthylen-Schmelzen, Rheol. Acta, 10, 230-242, 1971. https://doi.org/10.1007/BF02040447.

[12] J. Meissner, T. Raible, S.E. Stephenson, Rotary clamp in uniaxial and biaxial extensional. rheometry of polymer melts. J. Rheology 25:1-28, 1981. https://doi.org/10.1122/1.549612

[13] L. Li, T. Masuda, M. Takahashi, Elongational flow behavior of ABS polymer melts, J. Rheol. 34, 103-116, 1990. https://doi.org/10.1122/1.550112.

[14] J. Meissner, S.E. Stephenson, A. Demarmels, P. Portmann, Multiaxial elongational flows of polymer melts classification and experimental realization, J. Non-Newtonian Fluid Mech. 11, 221-237, 1982. https://doi.org/10.1016/0377-0257(82)80031-1.

[15] J. Meissner, Experimental aspects in polymer melt elongational rheometry, Chem. Eng. Commun. 33, 159-180, 1985. https://doi.org/10.1080/00986448508911167.

[16] S. Kawabata, H. Kawai, Strain energy density functions of rubber vulcanizates from biaxial extension, Adv. Polym. Sci. 24, 89-124, 1977. https://doi.org/10.1007/3-540-08124-0_2.

[17] G.H. Menary, C.G. Armstrong, R.J. Crawford, and J.P. McEvoy, Biaxial deformation and experimental study of PET at conditions applicable to stretch blow molding. Polymer Engineering and Science, 52 (3), pp. 671-688, 2012.

[18] M. Ru, X.Q. Lei, X.M. Liu, Y.J. Wei. An Equal-Biaxial Test Device for Large Deformation in Cruciform Specimens. Experimental Mechanics 62:677–683, 2022. https://doi.org/10.1002/pen.22134.

[19] P. Chandran, S. Jabarin, Biaxial orientation of poly (ethylene terephthalate). Part II: The strain–hardening parameter. Adv Polym. Technol. 12 (2), 119–132, 1993. https://doi.org/10.1002/adv.1993.060120203.

[20] P. Chandran, S. Jabarin, Biaxial orientation of poly(ethylene terephthalate). Part I: Nature of the stress—strain curves. Adv Polym. Technol. 12 (2), 133–151, 1993. https://doi.org/10.1002/adv.1993.060120202.

[21] E. Gorlier, J.F. Agassant, J.M. Haudin, N. Billon. Experimental and theoretical study of uniaxial deformation of amorphous poly(ethylene terephthalate) above glass transition temperature. Plast. Rubber Compos., 30, pp. 48-55, 2001. https://doi.org/10.1179/146580101101541435.

[22] L. Chevalier, Y. Marco, Identification of a strain induced crystallisation model for PET under uni- and bi-axial loading: Influence of temperature dispersion. Int. J. Mech. Mater., 39(6), 596–609, 2006. https://doi.org/10.1016/j.mechmat.2006.09.001.

[23] C.P. Buckley, D.C. Jones, Hot-drawing of poly(ethylene terephthalate) under biaxial stress: application of a three-dimensional glass—rubber constitutive model. Polymer, 37, 2403 -2414, 1996. https://doi.org/10.1016/0032-3861(96)85352-3

[24] W. Muller, K. Pohlant, New experiments for determining yield loci of sheet metal, Journal of material processing technology 60, 643-648, 1996. https://doi.org/10.1016/0924-0136(96)02399-0.

[25] M. Teaca, I. Charpentier, M. Martiny, G. Ferron, Identification of sheet metal plastic anisotropy using heterogeneous biaxial tensile tests. International Journal of Mechanical Sciences 52, 572–580, 2010. https://doi.org/10.1016/j.ijmecsci.2009.12.003.

[26] A. Makinde, L. Thibodeau, K. Neale, Development of an apparatus for biaxial testing using cruciform specimens. Experimental Mechanics, 32, 138-144, 1992. https://doi.org/10.1007/BF02324725.

[27] Demmerle, S., Boehler, J.P., Optimal design of biaxial tensile cruciform specimens. J. Mech. Phys. Solids 41 (1), 143-181, 1993. https://doi.org/10.1016/0022-5096(93)90067-P.

[28] T. Lagoda, E. Macha, W.A. Bedkowski, A critical plane approach based on energy concepts: application to biaxial random tension-compression high-cycle fatigue regime, International Journal of Fatigue, 21, 5, 431-443, 1999. https://doi.org/10.1016/S0142-1123(99)00003-1.

[29] J.S. Welsh, D.F. Adams, An experimental investigation of the biaxial strength of IM6/3501-6 carbon/epoxy crossply laminates using cruciform specimens. Composites: Part A, 33, 6, 829-839, 2002. https://doi.org/10.1016/S1359-835X(01)00142-7.

[30] D. Green, K. Neale S. Macewen, A. Makinde, Experimental investigation of the biaxial behaviour of an aluminum sheet. International Journal of Plasticity 20, 1677–1706, 2004. https://doi.org/10.1016/j.ijplas.2003.11.012.

[31] A. Makris, T. Vandenbergh, C. Ramault, D. Van Hemelrijck, E. Lamkanfi, W. Van Paepegem, Shape optimisation of a biaxially loaded cruciform specimen. Polymer Testing, 29(2), 216-223, 2010. https://doi.org/10.1016/j.polymertesting.2009.11.004.

[32] E. Lamkanfi, W. Van Paepegem, J. Degrieck, C. Ramault, A. Makris, D. Van Hemelrijck, Strain distribution in cruciform specimens subjected to biaxial loading conditions. Part 1: Two-dimensional versus three-dimensionalfiniteelement model. PolymerTesting, 29(1), 7-13, 2010. https://doi.org/10.1016/j.polymertesting.2009.08.009.

[33] E. Lamkanfi, W. Van Paepegem, J. Degrieck, C. Ramault, A. Makris, D. Van Hemelrijck, Strain distribution in cruciform specimens subjected to biaxial loading conditions. Part 2: Influence of geometrical discontinuities. Polymer Testing, 29(1), 132-138, 2010. https://doi.org/10.1016/j.polymertesting.2009.10.002.

[34] L. Chevalier, Y.M. Luo, E. Monteiro, G. Menary, On Visco-elastic Modelling of the Poly Ethylene Terephthalate Behaviour during Multiaxial Elongations Slightly over the Glass Transition Temperature, Mechanics of Material, Volume 52, p103 - 116, 2012. https://doi.org/10.1016/j.mechmat.2012.05.003.

[35] Y. M. Luo, L. Chevalier, F. Utheza, E. Monteiro, Numerical simulation of the thermodependant viscohyperelastic behavior of polyethylene terephthalate near the glass transition temperature: Prediction of the self-heating during biaxial tension test. Polymer Engineering and Science, 53(12), 2683-2695, 2013. https://doi.org/10.1002/pen.23522.

[36] Y.M. Luo, L. Chevalier. On Induced Properties and Self Heating during Free Blowing of PET Preform. International Polymer Processing, 34(3), P330-338, 2019. https://doi.org/10.3139/217.3759.

[37] F. Brezzi, M. Fortin, Mixed and hybrid Finite Element Methods, Springer-Verlag, Berlin, Heidelberg, 1991.

[38] O.C. Zienkiewicz. The finite element method. Volume1: The Basis. Butterworth-Heinemann, 2000.

[39] T.T. Nguyen, Y.M. Luo, L. Chevalier, F. Lesueur. Stochastic simulation of top load test on poly(ethylene terephthalate) bottles: An experimental study on dispersion of elastic properties. Journal of Applied Polymer Science, Wiley, pp.50837, 2021. https://doi.org/10.1002/app.50837.

Highlights

- A new vertical and transportable biaxial testing device including thermal regulation is designed and built up. The heating system provides quickly a homogeneous temperature of the specimen.
- A cruciform specimen shape is optimized reach high level of strain (up to 200%).
- An identification procedure of a viscohyperelastic model coupled with temperature is performed from equal-biaxial tensile results.

Graphical abstract